Int. J. Heat Mass Transfer. Vol. 35, No. 1, pp. 111–120, 1992
Printed in Great Britain

0017–9310/92 $5.00 + 0.00

Thermal convection loop with heating from above

Y.-Z. WANG and HAIM H. BAU†
Department of Mechanical Engineering and Applied Mechanics, University of Pennsylvania, Philadelphia, PA 19104-6315, U.S.A.

(*Received* 14 *December* 1990 *and in final form* 11 *February* 1991)

Abstract—The dynamics of single phase, buoyancy-induced flow in a toroidal loop are investigated theoretically under conditions of time-dependent, periodically varying, wall temperature. The heating and cooling, which are applied to the loop walls, are symmetrical with respect to the loop's axis which is parallel to the gravity vector. On average, the upper half's temperature is maintained at a higher value than that of the lower half. That is, on average, the temperature field inside the loop is stably stratified and the Rayleigh number based on the average temperature difference assumes a negative value. Despite this fact, as the Rayleigh number decreases, the flow in the loop exhibits a rich range of flow structures with a net amount of heat transport from the hot to the cold boundary. As the Rayleigh number decreases, the flow structures change from no-motion to time periodic motion to chaotic flow occasionally interrupted by periodic windows.

1. INTRODUCTION

THERMAL convection loops provide a means for circulating fluid without the use of pumps. Such loops are of interest for solar heaters, emergency reactor-core cooling, and process industries. They are also of interest for the understanding of warm springs, seawater circulation in the oceanic crust, and the formation of ore deposits. Most of the work to date has focused on dynamics of the flow in loops subject to time-independent boundary conditions. Due to the vast amount of literature on thermal convection loops, we cite below only a sample of the most relevant articles. For additional references, the reader is referred to review articles by Metrol and Greif [1] and Bau and Wang [2] and the literature cited therein.

Toroidal thermal convection loops with symmetrical wall temperature distributions and time-independent boundary conditions have attracted considerable attention in the scientific literature. Malkus [3] showed that for time-independent wall temperatures, the partial differential equations describing the cross-sectionally averaged flow in the loop can be reduced, with exact closure, to three ordinary differential equations similar to the Lorenz equations. The Lorenz equations were originally derived in a celebrated paper by Lorenz [4] as a crude approximation for Bénard convection. Since then, these equations have been investigated intensively (i.e. Sparrow's book [5]). Malkus' treatment has been expanded by Hart [6, 7] to include more general friction and heat transfer coefficients. The theoretical model predicts various flow structures which for moderate and large loop Prandtl numbers include, in order of increasing Rayleigh number: no-motion, steady motion, chaos (which is occasionally interrupted by periodic windows) and periodic flow [8]. For small Prandtl numbers, there are no time-dependent flows. These theoretical predictions have been partially confirmed by experimental observations. Khlebutin and Shaidurov [9] obtained heat transfer correlations for steady convection but did not observe any time-dependent flows. Creveling *et al.* [10] studied the stability of the steady motion theoretically and experimentally. They observed that as the Rayleigh number increases, the steady convection is replaced with time-dependent, aperiodic flow with occasional reversals in the flow direction. Similar results have been reported by Ehrhard and Muller [11]. Gorman *et al.* [12] have focused on the chaotic nature of the time-dependent flow. During the last few years, we have been operating, at the University of Pennsylvania [13], a thermal convection loop similar to the one constructed by Creveling *et al.* [10] as an experimental demonstration of chaotic dynamics.

Most of the work to date has focused on convective processes with time-independent wall conditions. Far fewer studies address the stability of time-dependent convection. However, in many processes in industry and nature, the boundary conditions are not fixed in time. As we shall demonstrate, time-wise variations of boundary conditions may give rise to new and sometimes unexpected physical phenomena. The effect of time-dependent boundary conditions is also of interest when exploring the feasibility and means of controlling the flow in the loop (i.e. promoting or retarding chaos) through boundary perturbations. For example, in a related study [14], we used an active (feedback) controller to suppress (laminarize) chaotic motion which naturally occurs in our loop at sufficiently high Rayleigh numbers. For these reasons, we study the effect of time-dependent wall temperatures on the dynamics of thermal convection. In an earlier

† Author to whom correspondence should be addressed.

paper [15], we described the flow dynamics in a loop heated from below with time periodic wall temperature. Briefly, we observed in sequence of increasing Rayleigh number, a no-motion state, periodic motion, chaotic motion and periodic motion. Depending on the magnitude of the loop's Prandtl number and the modulation's amplitude, transition to chaos occurred either through a period doubling sequence or through a homoclinic explosion. In the case of periodic heating from above, since, on the average, the thermal field is stably stratified, one would expect that the flow behavior would be relatively simple. Our present investigation indicates that this is not necessarily the case. Indeed, one may observe a range of complicated flow structures which include periodic and chaotic motions.

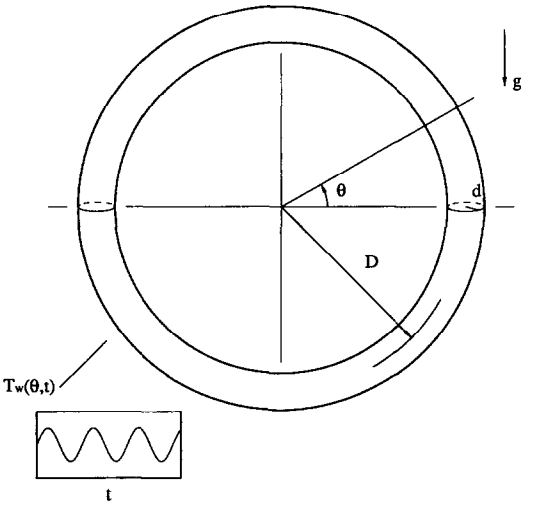

FIG. 1. Schematic description of the thermal convection loop.

2. MATHEMATICAL MODEL

Consider a fluid filled pipe of inner radius d bent to form a torus of radius $D \gg d$. The wall temperature of the pipe $T_w(\theta, t)$ may vary with the angular location θ and time t (Fig. 1). The cross-sectionally averaged temperature variations $T(\theta, t)$ in the loop may induce fluid motion of cross-sectionally-averaged velocity $u(t)$. The fluid is assumed to be incompressible and Newtonian. Within the framework of Boussinesq's approximation, the dimensionless mass, momentum and energy conservation equations are [16]

$$u = u(t) \tag{1}$$

$$\dot{u}(t) = \frac{1}{\pi} RP \oint T(\theta, t) \cos(\theta)\, d\theta - Pu(t) \tag{2}$$

and

$$\dot{T}(\theta, t) = -u(t)\frac{\partial T(\theta, t)}{\partial \theta} + B\frac{\partial^2 T(\theta, t)}{\partial \theta^2} + [T_w(\theta, t) - T(\theta, t)]. \tag{3}$$

In the above, $R = g\beta\Delta T\tau^2/(2DP)$ is the loop's Rayleigh number; β the fluid's thermal expansion coefficient; g the gravitational acceleration; and ΔT the time-averaged, wall temperature difference between the loop's bottom and top. In this paper $\Delta T < 0$, thus $R < 0$. The time scale is $\tau = \rho C_p d/2h$, where ρ is the average fluid density, C_p the heat capacity, and h (which we assume to be constant) the heat transfer coefficient between the fluid and the pipe wall. $P = 4\nu\tau/d^2 = 8Pr/Nu$ is the loop's Prandtl number; ν the kinematic viscosity; and $Pr = \nu/\alpha$ and $Nu = 2hd/k$ the conventional Prandtl and Nusselt numbers, respectively. α and k are the fluid's thermal diffusivity and conductivity; and $B = 1/Nu(d/D)^2$ the Biot number. The length scale is the loop's radius D.

In addition to the aforementioned Boussinesq approximation, the aforedescribed mathematical model assumes implicitly that the friction and heat transfer laws are similar to those of laminar, fully developed, Poiseuille pipe flow. One would expect and we did, in fact, observe in experiments the development of secondary circulation which may significantly modify both the friction and heat transfer laws. More realistic friction and heat transfer laws are not known a priori. To obtain these correlations, one may need to solve a spatially three-dimensional model or conduct experiments. We justify the use of the simpler correlations on the grounds that this simple model still provides a qualitatively correct picture as has been confirmed by our own experiments [14] and those by others [11, 12] for loops with time-independent wall temperature.

Equations (1)–(3) constitute a set of non-linear differentio-integral equations for which, in general, an exact solution is not available. We expand the wall and fluid temperatures in Fourier series in terms of the angle θ

$$T_w(\theta, t) = W_0(t) + \sum_{n=1}^{\infty} W_n(t) \sin(n\theta) \tag{4}$$

and

$$T(\theta, t) = \sum_{n=0}^{\infty} S_n(t) \sin(n\theta) + C_n(t) \cos(n\theta). \tag{5}$$

Upon substituting the series (4) and (5) into the governing equations (1)–(3) and requiring that these equations are satisfied in the sense of weighted residuals, we obtain an infinite set of ordinary differential equations. It turns out that three equations in the set decouple from the rest of the set and can be solved independently of the other equations without need for truncation. Thus, the full dynamics of the problem (1)–(3) are contained in the three equations

$$\dot{u} = P(c - u) \tag{6}$$

$$\dot{c} = -us - c \tag{7}$$

$$\dot{s} = uc - s - R[1 + \varepsilon \sin(\omega t)]. \quad (8)$$

Once these three equations are integrated, the remaining set of (slaved) equations can be solved as well. In the special case of $\varepsilon = 0$, equations (6)–(8) reduce to the celebrated Lorenz [4] equations. In the above, we removed the dependence on the Biot number, B, via the simple, algebraic transformation $\{u, C, S, R, P, t\} \to 1/(1+B)\{u, RC_1, RS_1, R/(1+B), P, t\}$ and prescribed the wall temperature to vary periodically with time, i.e. $W_1 = 1 + \varepsilon \sin(\omega t)$.

Equations (6)–(8) are nonlinear and admit a number of possible solutions. Depending on the magnitude of the system's parameters, these are no-motion, periodic and chaotic motions.

3 THE NO-MOTION SOLUTION AND ITS STABILITY

Equations (6)–(8) admit a no-motion, long term, $T(= 2\pi/\omega)$ periodic solution of the form

$$\{u, c, s\} = \{0, 0, -R[1 + \varepsilon/\varepsilon_0 \sin(\omega t + \phi)]\} \quad (9)$$

where $\varepsilon_0 = \sqrt{(1+\omega^2)}$ and $\phi = \arcsin(-\omega/\varepsilon_0)$. The terminology 'no-motion' implies here the absence of net circulation in the loop. The thermal interaction between the fluid and the pipe's walls causes the fluid's temperature to oscillate at the same period as the wall temperature, albeit with a phase lag (ϕ). When $\varepsilon \to 0$ and/or $\omega \to \infty$, the fluid's temperature is fixed in time and the solution is identical to that of the unmodulated loop (the classical Lorenz equations).

In the subsequent derivation, it is convenient to introduce a set of new variables $\{X, Y, Z\}$ such that

$$\{u, c, s\} = \{X, Y, Z - R[1 + \varepsilon/\varepsilon_0 \sin(\omega t + \phi)]\}. \quad (10)$$

In terms of these new variables, the no-motion solution corresponds to the origin of the phase space $\{X, Y, Z\}$ and equations (6)–(8) assume the form

$$\dot{X} = P(Y - X) \quad (11)$$

$$\dot{Y} = RX\left[1 + \frac{\varepsilon}{\varepsilon_0} \sin(\omega t + \phi)\right] - Y - XZ \quad (12)$$

$$\dot{Z} = -Z + XY. \quad (13)$$

Next, we investigate the linear stability of the no-motion state. To this end, we drop the non-linear terms in equations (11) and (12) to obtain a set of linear differential equations with periodic coefficients. It is immediately apparent that

$$\lim_{t \to \infty} Z(t) = 0.$$

The remaining two equations constitute the damped Mathieu system

$$\dot{X} = P(Y - X) \quad (14)$$

$$\dot{Y} = RX\left[1 + \frac{\varepsilon}{\varepsilon_0} \sin(\omega t + \phi)\right] - Y. \quad (15)$$

Floquet theory suggests that the solutions of this linearized system can be presented in the form $\{X, Y\} = \{x, y\} \exp(\sigma t)$, where $\{x, y\}$ are T periodic functions and σ is the Floquet exponent. The spectral problem of stability involves the determination of the critical R values which correspond to $\mathrm{Re}\{\sigma\} = 0$. In Fig. 2, we depict this critical value as a function of the disturbance amplitude ε for the loop's Prandtl number $P = 4$ and forcing frequency $\omega = 1$. That is, the period of the forcing is comparable in magnitude to the thermal equalization time between the temperatures

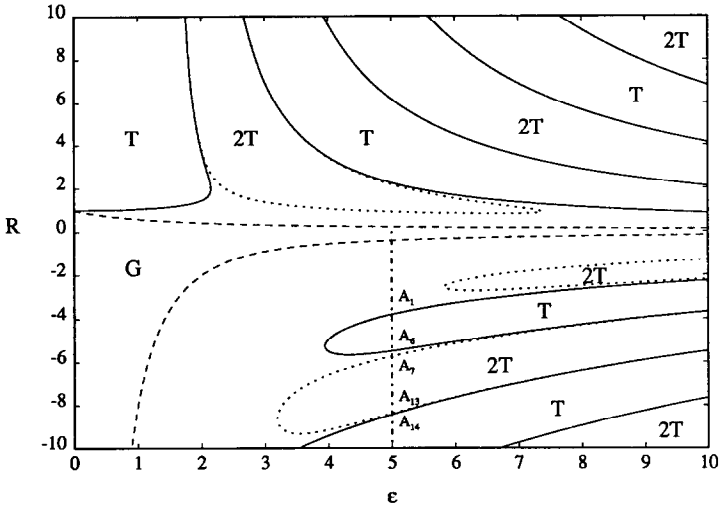

FIG. 2. Stability diagram for the no-motion state for $p = \omega = 1$. The Rayleigh number at the onset of convection as predicted by linear stability analysis is depicted as a function of the modulation amplitude (ε). The symbols T and $2T$ indicate, respectively, bifurcation into harmonic (T periodic) and subharmonic ($2T$ periodic) motion solutions. The region (G) indicates global stability. The vertical line at $\varepsilon = 5$ corresponds to the bifurcation diagram shown in Fig. 3.

of the fluid and the wall. The upper half and lower half of Fig. 2 correspond, respectively, to positive (heating from below) and negative (heating from above) Rayleigh numbers. The symbols T and $2T$ in Fig. 2 indicate bifurcation into T (harmonic) and $2T$ (subharmonic) flows. That is, depending on the magnitude of ε, the no-motion solution may bifurcate to either T (same frequency as the forcing) or $2T$ (half forcing frequency) periodic flow. For each value of the Rayleigh number, there are two solutions which correspond, respectively, to motion predominantly in the clockwise or the counterclockwise directions.

In this paper, we focus on negative R. From Fig. 2, we observe that for small negative R, the no-motion solution is linearly stable. The region of stability decreases as ε increases. In the next section, we shall follow the chain of events as R decreases for a fixed ε ($= 5$, say). This corresponds to the vertical dashed line depicted in Fig. 2. Following this line, we observe that the no-motion solution loses stability at point A_1 (the symbols A_i are cross-referenced with Fig. 3) in favor of a T periodic motion (whose stability characteristics are determined in the next section). As we further decrease R, the no-motion solution regains stability in the intervals A_6–A_7 and A_{13}–A_{14}. That is, if we were to conduct an experiment in which we gradually decreased R, we would observe initially a no-motion state, then motion states (which we describe later in detail) and the occasional reappearance of no-motion states corresponding to the areas between the 'fingers' in Fig. 2.

The linear stability analysis (Fig. 2) indicated at which values of R the no-motion solution loses its stability because of small disturbances. This analysis, however, does not provide information on the size of the basin of attraction of the no-motion solution. To this end, we resort to global analysis.

To obtain estimates of the global stability of the no-motion solution, we use the method of Lyapunov. As we focus in this paper on heating from above, we shall construct the global stability limits only for $R < 0$. A similar technique can be used for $R > 0$ [17]. Briefly, we construct the positive definite Lyapunov functionals

$$E_1 = \frac{1}{2}\left\{-\frac{R}{P}X^2 + Y^2 + Z^2\right\} \quad \text{for} \quad 0 \leqslant \frac{\varepsilon}{\varepsilon_0} < 2$$

$$E_2 = \frac{1}{2}\left\{\frac{1}{P}X^2 + Y^2 + Z^2\right\} \quad \text{for} \quad 2 < \frac{\varepsilon}{\varepsilon_0} \leqslant \infty \quad (16)$$

whose time derivatives

$$\dot{E}_1 = -\{-RX^2 + Y^2 + Z^2\} + RXY\frac{\varepsilon}{\varepsilon_0}\sin(\omega t + \varphi) \quad \text{for} \quad 0 \leqslant \frac{\varepsilon}{\varepsilon_0} < 2$$

$$\dot{E}_2 = -\{X^2 + Y^2 + Z^2\} + XY\left\{1 + R\left[1 + \frac{\varepsilon}{\varepsilon_0}\sin(\omega t + \varphi)\right]\right\} \quad \text{for} \quad 2 < \frac{\varepsilon}{\varepsilon_0} \leqslant \infty \quad (17)$$

must be negative to assure global stability (regardless of disturbance size). This is satisfied by

$$0 \geqslant R > -4\left(\frac{\varepsilon_0}{\varepsilon}\right)^2 \quad \text{for} \quad 0 \leqslant \frac{\varepsilon}{\varepsilon_0} < 2$$

and

$$0 \geqslant R > \frac{\varepsilon_0}{\varepsilon_0 - \varepsilon} \quad \text{for} \quad 2 < \frac{\varepsilon}{\varepsilon_0} \leqslant \infty \quad (18)$$

which yields for $\varepsilon \to 0$, the low bound of $R > -\infty$. The region in which global stability is guaranteed is denoted G in Fig. 2. In contrast to the linear stability limits, the global stability limits (18) do not depend on the frequency ω. Since the aforeselected Lyapunov functional (16) may not be optimal, the shown global stability limits may be conservative. We do know, however, that, in this case, the linear and global stability limits do not coincide as we find multiple solutions in regions predicted to be stable by linear theory. That is, in regions between the linear and global stability limits, the no-motion solution may have only a finite domain of attraction about whose size we shall comment in the next section.

4. MOTION SOLUTIONS

Next, we follow the chain of events as the Rayleigh number R decreases for a fixed ε ($= 5.0$, say). That is, we follow the dashed, vertical line in Fig. 2. In Fig. 3, we show the fluid's velocity (X) as a function of R for $\varepsilon = 5$, $\omega = P = 1$. In order to obtain the bifurcation diagram depicted in Fig. 3, we used numerical tools. We integrated the loop equations (11)–(13) using a fourth-order accurate Runge–Kutta scheme and employed standard procedures [5] to locate periodic orbits and study their stability. Figure 3 was constructed by probing the velocity (X) stroboscopically with period T. Thus, in Fig. 3, a single point at a given R indicates a T periodic motion; two points indicate a subharmonic with period $2T$; N points indicate a subharmonic with period NT; and a smear of points indicates chaotic behavior. Stable and non-stable solutions in Fig. 3 are denoted, respectively, with solid and dashed lines.

The loop equations (11)–(13) are invariant under the transformation $\{X, Y, Z, t\} \leftrightarrow \{-X, -Y, Z, t\}$. Consequently, we expect to find two types of solutions: one type, entitled 'symmetric', which satisfies the aforementioned invariance (i.e. the trajectory associated with the symmetric solution will pass through both points $\{X_1, Y_1, Z_1\}$ and $\{-X_1, -Y_1, Z_1\}$ in phase space); and a second type of solution, entitled asymmetric, which does not obey the aforementioned invariance. Asymmetric solutions always appear in pairs. Each asymmetric solution has a mirror image which we do not show in Fig. 3.

The point denoted A_1 in Figs. 2 and 3 corresponds to the loss of stability of the no-motion solution. As the bifurcation is subcritical, the resulting T periodic, asymmetric motion solution (A_1–A_2) is non-stable for

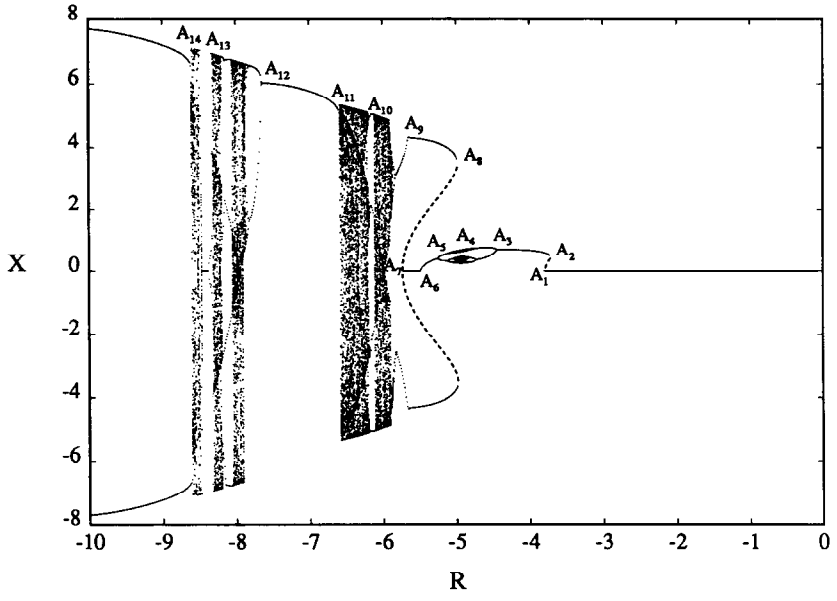

FIG. 3. A bifurcation diagram depicting the various flow regimes as a function of Rayleigh number. The diagram was generated by probing the velocity (X) stroboscopically with period T. N points at a given R indicates an NT periodic motion. A smear of points indicates chaotic behavior.

small (R–R_{A_1}) [18]. This non-stable solution gains stability at the turning point A_2 in Fig. 3 resulting in a stable T periodic motion (Fig. 4) in the interval A_2–A_3. In the region A_1–A_2, there are three possible solutions: the stable, no-motion solution ($X = 0$); the stable T periodic, motion solution and the non-stable, T periodic, motion solution. The non-stable solution (A_1–A_2) provides a boundary between the basins of attraction of the stable no-motion and motion solutions. Note also the hysteresis phenomenon encountered at points A_1 and A_2. That is, if one had conducted an experiment in which R is gradually

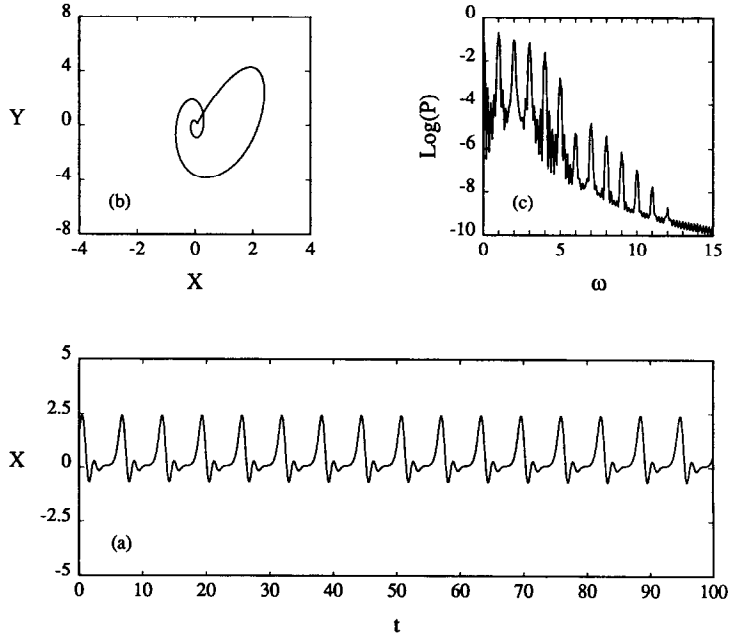

FIG. 4. The T periodic, stable motion solution in the interval A_2–A_3 in Fig. 3. The velocity X as a function of time (t), the motion trajectory projected on the XY plane, and the spectrum of X in the frequency domain are shown, respectively in (a)–(c).

decreased, one would observe a discontinuous jump in X at point A_1 from a no-motion state to a T periodic motion. If a similar experiment were conducted with increasing R, the discontinuous jump would occur at point A_2 from T periodic motion to no-motion.

The stable T periodic, motion solution existing in the interval A_2–A_3 is depicted in Fig. 4. Figures 4(a)–(c) show, respectively, the velocity X as a function of the time t, the XY projection of the motion-trajectory in phase space, and the spectrum of the signal $X(t)$. As the motion is periodic, the trajectory describes a closed curve in phase space. The spectrum reveals dominating frequencies which are all integer multiples of the forcing frequency ($\omega = 1$) consistent with a periodic motion. Even though the loop is, on average, stably stratified, the oscillations result in flow with a non-zero mean, as is apparent from the time series in Fig. 4. Thus, we can expect net convective heat transport from the hot, upper half to the cold, lower half. This is shown in Fig. 5, which depicts the time average convective transport

$$\overline{XY} = \lim_{\tau \to \infty} \frac{1}{\tau} \int_0^\tau X(t) Y(t)\, dt$$

as a function of the Rayleigh number. For clarity, only one solution branch is shown in Fig. 5.

At point A_3 in Fig. 3, the T periodic solution loses stability and undergoes a supercritical period doubling bifurcation into a stable $2T$ periodic solution whose trajectory projected on the XY plane is depicted in Fig. 6(a). Note that the trajectory has a similar structure to the one shown in Fig. 4 with the curve being doubled. The period doubling sequence continues in quick succession (the resolution of Fig. 3 allows us to see only up to the $8T$ periodic solution) until it terminates with the appearance of an asymmetric, chaotic window at A_4. The XY projection of the trajectories corresponding to the chaotic motion is shown in Fig. 6(b). Although the trajectories in Fig. 6(b) do not repeat themselves, the phase space portrait appears to have a distinct structure. That is, the orbits tend to spend most of the time within well defined tubes in phase space. This type of chaotic behavior was entitled by Lorenz [19] noisy (semi) periodicity. We shall describe noisy periodicity in more detail when we discuss another chaotic attractor later on in the paper.

The chaotic window disappears through a reversed period doubling sequence which terminates with a T periodic solution at A_5. As the Rayleigh number is further decreased, the amplitude of the T periodic solution decreases to zero at A_6. At this point, the no-motion solution regains stability and remains stable within the interval A_6–A_7. The interval A_6–A_7 corresponds to the gap between the T and $2T$ periodic solutions in Fig. 2. This no-motion solution undergoes a subcritical bifurcation at point A_7 into a non-stable, symmetric $2T$ periodic solution (consistent with the predictions of the linear stability analysis, Fig. 2). The $2T$ periodic solution regains stability at the turning point A_8. The situation at point A_7 is similar to that at A_1 in the sense that we encounter the co-existence of multiple solutions and a hysteresis phenomenon.

The symmetric, $2T$ solution remains stable in the interval A_8–A_9. At A_9, it undergoes a symmetry breaking bifurcation into an asymmetric, stable $2T$ solution. As the Rayleigh number is further reduced, the $2T$ periodic solution undergoes a sequence of period doublings which terminates in a symmetric chaotic attractor. The chaotic behavior is depicted in terms of the time series X vs t and the corresponding power spectrum in Figs. 7 and 8. The XY projection of the trajectories is shown in Fig. 9. The time series (Fig. 7) consists of non-periodic bursts of motion either in the clockwise or counterclockwise direction interrupted by intervals of low velocity ($X \sim 0$). The

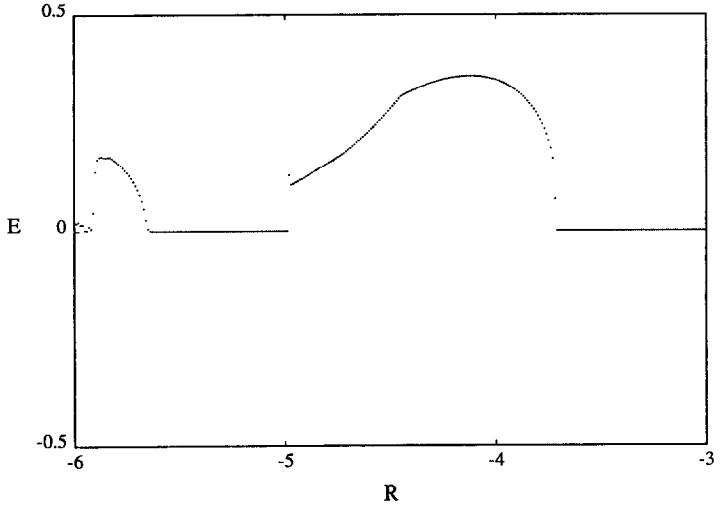

FIG. 5. The average convected energy is depicted as a function of the Rayleigh number (R).

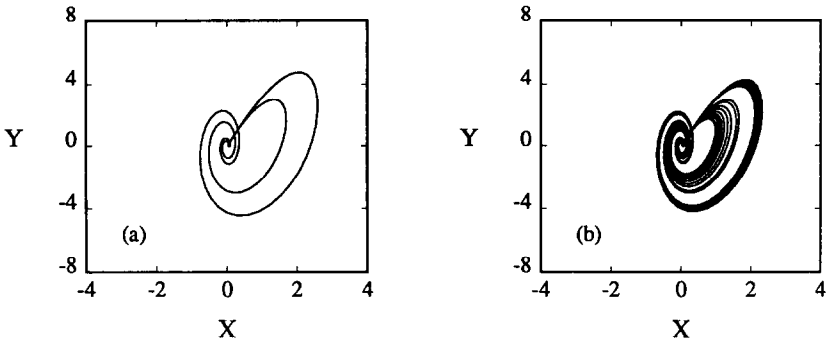

FIG. 6. XY projection of the phase portrait for (a) $2T$ periodic solution at $R = -4.6$ and (b) the chaotic attractor at $R = -4.9$.

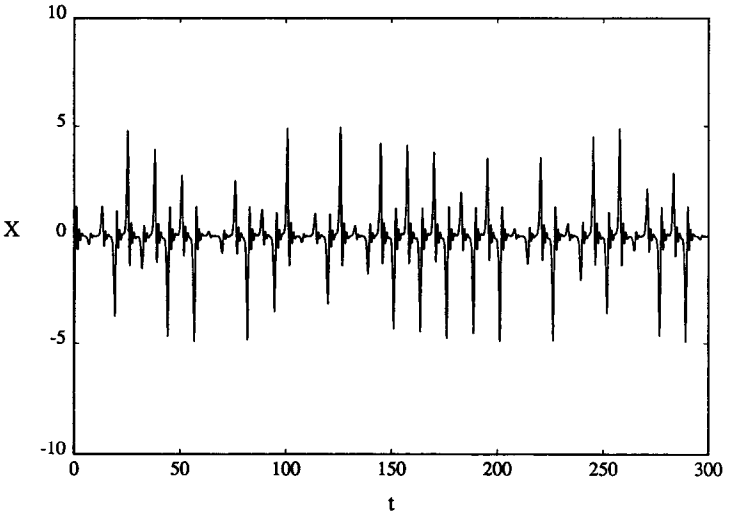

FIG. 7. The velocity (X) shown as a function of time in the chaotic regime ($R = -6$).

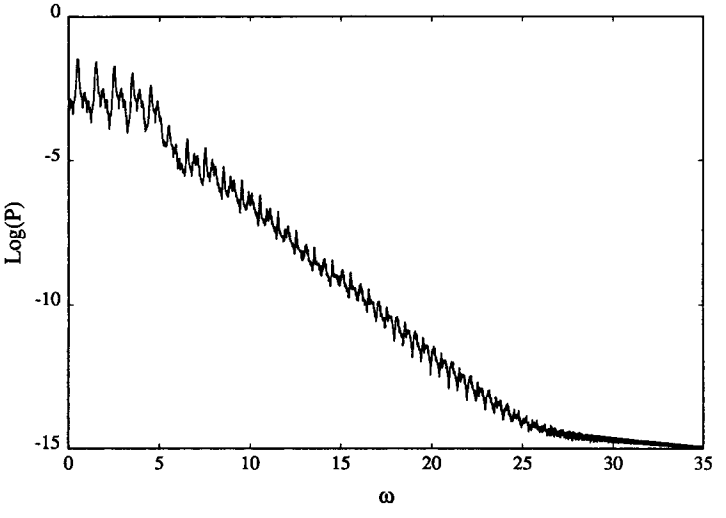

FIG. 8. The power spectrum of the chaotic signal at $R = -6$.

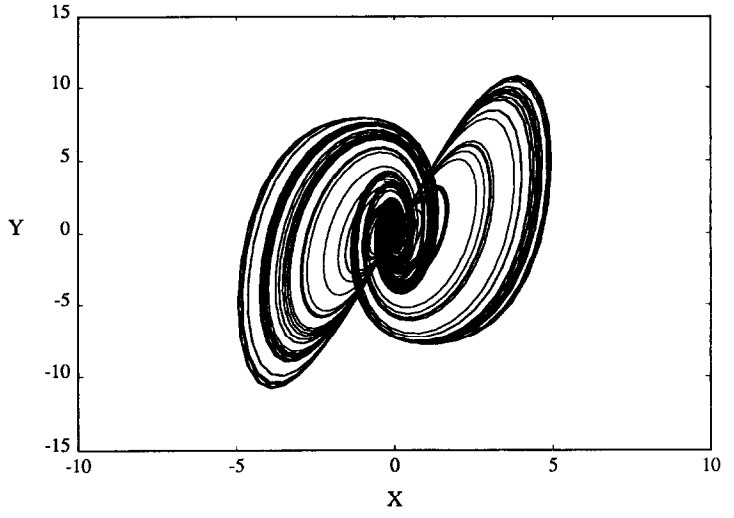

FIG. 9. XY projection of the phase portrait of the chaotic attractor at $R = -6$.

power spectrum depicted in Fig. 8 exhibits a few broad-band areas around dominating frequencies at $\omega_i \sim 0.5$, 1.5, 2.5 and 3.5, which are not integer multiples of the forcing frequency. The power spectrum and the attractor's structure suggest that the chaotic behavior exhibits noisy or (semi) periodicity. The attractor (Fig. 9) appears to have the relatively simple structure of a plane bent into a saddle-shape. This view of the attractor is further enhanced when we examine the Poincare cross-section of the attractor (Fig. 10).

We define Poincare cross-sections as R^3 hypersurfaces with Mod $(t, T) = (m/n)T$, where $0 \leqslant m < n$, and n are integers. By using Poincare sections, we transform the continuous time system to a discrete system. Since it may be inconvenient to depict higher-order dimensional surfaces, we shall resort to projections onto lower dimensional hypersurfaces. For example, in Fig. 10, we show an XY projection of the Poincare section which appears as a single S-shaped line. The appearance of a single curve is the result of insufficient resolution of the figure and it attests to the strong contraction of the attracting set in the direction normal to the curve. This contraction is a result of the dissipative nature of the equations which causes trajectories to contract volume in phase space. In actuality, the curve in Fig. 10 consists of many layers bounded close together. The dynamics of the attractor can be studied conveniently through a return map (Fig. 11). The return map is constructed by taking a set of points $\{X_n\}$ at some time t and finding their corresponding values $\{X_{n+1}\}$ at time $t+T$. The map

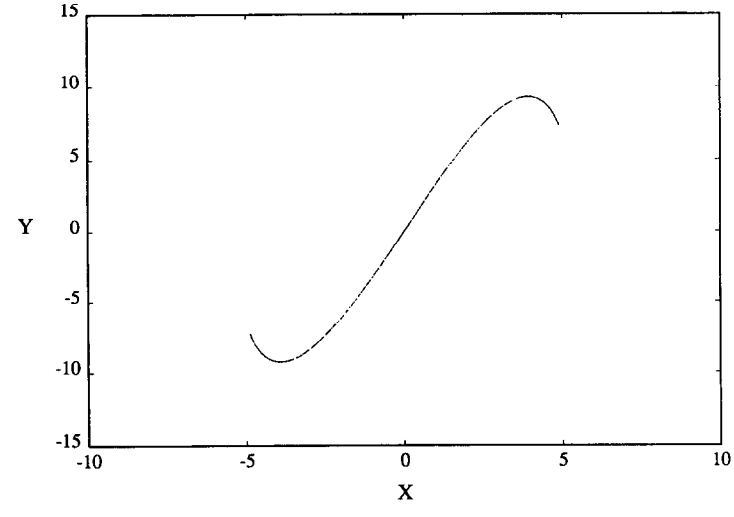

FIG. 10. XY projection of the Poincare cross-section of the chaotic attractor at $R = -6$.

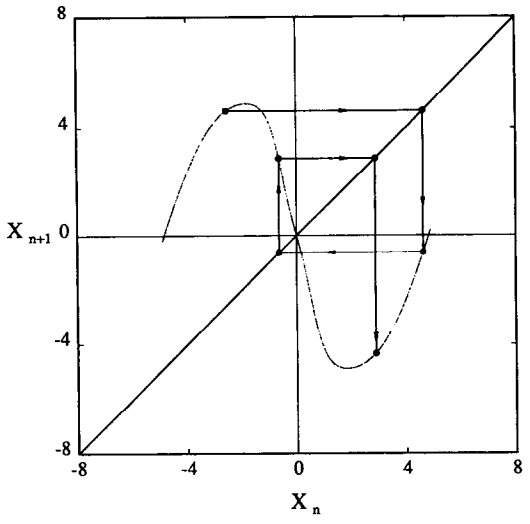

FIG. 11. A return map describing the dynamics on the chaotic attractor ($R = -6$).

in Fig. 11 also includes a 45° (dashed) line which will assist us in the construction of the motion trajectories. The dynamics of the attractor can be studied by selecting any point on the return map (X_1, say), drawing a horizontal line to the 45° line and erecting a vertical line to the return map to find point X_2, etc. Note that the return map suggests a change in the sign of X (the flow direction) at every iteration (within every period T).

The chaotic attractor is interrupted with a periodic window at A_{10} (Fig. 3) and is terminated at A_{11} by a saddle node bifurcation into a T periodic solution. The periodic solution is visible in the chaotic regime and it appears to bifurcate supercritically from the non-stable no-motion solution. This T periodic solution undergoes a period doubling sequence which results in another chaotic region with periodic windows. Realizing that the analysis could go on indefinitely, we decided to terminate it at this point.

5. CONCLUSION

We analyzed the behavior of a thermal convection loop subjected, on average, to heating from above. Although the temperature field in the loop is on average stably stratified, we observed, contrary to what one might expect, that as the Rayleigh number decreases, a large number of complicated flow structures, ranging from no-motion to periodic motion with various periodicities to chaos, occur. It is interesting to note that the motion solutions consist of motion pulses with intervals of almost no-motion in between. The results also indicate that, in spite of the stable stratification (on the average), net circulation of mass and energy is possible. The results may be of interest, among other things, to circulation in the ocean and the earth where upper surfaces are subject to periodic temperature fluctuations.

Acknowledgement—This work was supported by the National Science Foundation (Grant CBT 83-51658).

REFERENCES

1. A. Metrol and R. Greif, A review of natural circulation loops. In *Natural Convection: Fundamentals and Applications* (Edited by W. Aung, S. Kakac and R. Viskanta). Hemisphere, New York (1985).
2. H. H. Bau and Y.-Z. Wang, Chaos: a heat transfer perspective. In *Annual Reviews of Heat Transfer IV* (Edited by C. L. Tien), pp. 1–50. Hemisphere, New York (1991).
3. W. V. R. Malkus, Non-periodic convection at high and low Prandtl number. In *Mémoires Societe Royale des Sciences de Liege*, Ser. 6, Vol. IV, pp. 125–128 (1972).
4. E. N. Lorenz, Deterministic nonperiodic flow, *J. Atmos. Sci.* **20,** 130–141 (1963).
5. C. Sparrow, *The Lorenz Equations: Bifurcations, Chaos, and Strange Attractors*. Springer, Berlin (1982).
6. J. E. Hart, A new analysis of the closed loop thermosyphon, *Int. J. Heat Mass Transfer* **27,** 125–136 (1984).
7. J. E. Hart, A note on the loop thermosyphon with mixed boundary conditions, *Int. J. Heat Mass Transfer* **28,** 939–947 (1985).
8. K. A. Robbins, Periodic solutions and bifurcation structure at high R in the Lorenz model, *SIAM J. Appl. Math.* **36,** 457–472 (1979).
9. G. N. Khlebutin and G. F. Shaidurov, Thermal convection in a vertical annular tube, *Inzh.-fiz. Zh.* **8,** 3–6 (1965).
10. H. F. Creveling, J. F. De Paz, J. Y. Baladi and R. J. Schoenhals, Stability characteristics of a single phase thermal convection loop, *J. Fluid Mech.* **67,** 65–84 (1975).
11. P. Ehrhard and U. Muller, Dynamical behavior of natural convection in a single-phase loop, *J. Fluid Mech.* **217,** 487–518 (1990).
12. M. Gorman, P. J. Widmann and K. A. Robins, Chaotic flow regimes in a convection loop, *Phys. Rev. Lett.* **52,** 2241–2244 (1984).
13. H. H. Bau, New, improved formula for an ME laboratory, *A.S.M.E. Mech. Engng* **111,** 84–87 (February 1989).
14. J. Singer, Controlling a chaotic system, M.Sc. Thesis, University of Pennsylvania (1991).

15. Y.-Z. Wang and H. H. Bau, Period doubling and chaos in a thermal convection loop with time periodic wall temperature variation, *Proc. Int. Heat Transfer Conf.*, Vol. II, pp. 357–362 (1990).
16. H. H. Bau and K. E. Torrance, Transient and steady behavior of an open, symmetrically-heated, free convection loop, *Int. J. Heat Mass Transfer* **24**, 597–609 (1981).
17. Y.-Z. Wang, Problems in thermal convection, Ph.D. Thesis, University of Pennsylvania, Philadelphia (1991).
18. G. Iooss and D. D. Joseph, *Elementary Stability and Bifurcation Theory*, 2nd Edn. Springer, Berlin (1989).
19. E. N. Lorenz, Noisy periodicity and reverse bifurcation. In *Nonlinear Dynamics* (Edited by R. H. G. Helleman), pp. 287–291. New York Academy of Sciences, New York (1980).

BOUCLE DE CONVECTION THERMIQUE AVEC CHAUFFAGE PAR DESSOUS

Résumé—La dynamique d'un écoulement monophasique induit par les forces de flottement dans une boucle toroïdale est étudiée théoriquement sous des conditions de température pariétale variant périodiquement dans le temps. Le chauffage et le refroidissement qui sont appliqués aux parois de la boucle sont symétriques par rapport à l'axe qui est parallèle au vecteur gravité. En moyenne, la température de la moitié supérieure a une valeur plus grande que celle de la moitié inférieure. Le champ de température dans la boucle est stratifié de façon stable et le nombre de Rayleigh basé sur la différence des températures moyennes a une valeur négative. En dépit de cela, lorsque le nombre de Rayleigh décroît l'écoulement dans la boucle montre une riche variété de structures avec un transport thermique net depuis la frontière chaude jusqu'à la froide. Quand le nombre de Rayleigh diminue, les structures passent depuis le repos à la périodicité, à l'écoulement chaotique occasionnellement interrompu par des fenêtres périodiques.

NATURUMLAUFSYSTEM MIT BEHEIZUNG VON OBEN

Zusammenfassung—Es wird die Dynamik einer einphasigen, vom Auftrieb verursachten Strömung in einem torusförmigen Kreislaufsystem unter der Bedingung von zeitabhängigen, periodisch veränderlichen Wandtemperaturen untersucht. Die Heizung und Kühlung an den Wänden des Kreislaufsystems ist symmetrisch zu dessen Achse, die parallel zur Richtung der Erdbeschleunigung verläuft. Im Durchschnitt wird die Temperatur der oberen Hälfte auf einem höheren Wert als in der unteren Hälfte gehalten. Das bedeutet, daß das Temperaturfeld im Inneren des Kreislaufs im Mittel stabil geschichtet ist und daß die Rayleigh-Zahl, die auf der mittleren Temperaturdifferenz beruht, einen negativen Wert annimmt. Entgegen dieser Tatsache weist die Strömung im Kreislauf bei abnehmender Rayleigh-Zahl eine große Vielfalt an Strömungsformen mit einem Nettowärmetransport vom warmen zum kalten Bereich auf. Mit abnehmender Rayleigh-Zahl wechseln die Strömungsformen von keiner Bewegung über zeitlich periodische Bewegung zu chaotischer Strömung, die gelegentlich durch periodische Abschnitte unterbrochen ist.

КОНТУР ТЕПЛОВОЙ КОНВЕКЦИИ ПРИ НАГРЕВЕ СВЕРХУ

Аннотация—Теоретически исследуется динамика однофазного свободно-конвективного течения в тороидальном контуре в условиях нестационарной периодически изменяющейся температуры стенок. Нагрев и охлаждение на стенках контура являются симметричными относительно его оси, параллельной вектору силы тяжести. В среднем в верхней части контура поддерживается более высокая температура, чем в нижней, т.е. температурное поле внутри контура устойчиво стратифицировано и число Рэлея, основанное на средней разности температур, принимает отрицательное значение. Несмотря на это с уменьшением числа Рэлея структура течения в контуре претерпевает различные изменения с явным преобладанием переноса тепла от нагретой границы к холодной. По мере уменьшения числа Рэлея структуры течения изменяются от отсутствия движения к периодическому движению, а затем к хаотическому потоку, случайным образом прерываемому периодическими интервалами.